Nonadiabatic excited-state dynamics of ReCl(CO)$_3$(bpy) in two different solvents

Adam Šrut,[a,b] Sebastian Mai,[c] Igor V. Sazanovich,[d] Jan Heyda,*[a,b] Antonín Vlček,[a,e] Leticia González,*[c] and Stanislav Záliš*[a]

We present a study of the excited states relaxation within the complex ReCl(CO)$_3$(bpy) (bpy = 2,2'-bypyridine) using a nonadiabatic TD-DFT dynamics on spin-mixed potential energy surfaces in explicit acetonitrile (ACN) and dimethylsulfoxide (DMSO) solutions up to 800 fs. ReCl(CO)$_3$(bpy) belongs to group of important photosensitizers which show ultrafast biexponential subpicosecond fluorescence decay kinetics. The choice of solvents was motivated by the different excited-state relaxation dynamics observed in our newly measured subpicosecond time-resolved IR (TRIR) experiments. Simulations of intersystem crossing (ISC) showed the development of spin-mixed states in both solvents. Transformation of time-dependent populations of spin-mixed states enabled to monitor the temporal evolution of individual singlet and triplet states, fitting of bi-exponential kinetics and simulate the time-resolved fluorescence spectra with only minor differences between solvents. Analysis of structural relaxation dynamics and solvent reorganization, employing time-resolved proximal distribution functions, pointed to the factors influencing the fluorescence time constants. Finally, we have shown that nonadiabatic dynamics simulations are promising approach for interpreting time resolved spectroscopic data and ultrafast photochemical reactivity.

^{a} *J. Heyrovský Institute of Physical Chemistry, Academy of Sciences of the Czech Republic, 182 23 Prague, Czech Republic. Tel: +420 26605 3268; E-mail: stanislav.zalis@jh-inst.cas.cz*

^{b} *Department of Physical Chemistry, University of Chemistry and Technology, Prague, 166 28 Prague, Czech Republic. Tel: +420 22044 4297; E-mail: jan.heyda@vscht.cz*

^{c} *Institute for Theoretical Chemistry, University of Vienna, Währinger Straße 17, 1090 Vienna, Austria. Tel: +43 1 4277 52750; E-mail: leticia.gonzalez@univie.ac.at*

^{d} *Central Laser Facility, Research Complex at Harwell, STFC, Rutherford Appleton Laboratory, Harwell Oxford, Didcot, Oxfordshire, OX11 0QX, United Kingdom.*

^{e} *Department of Chemistry, Queen Mary University of London, London E1 4NS, United Kingdom.*

† Electronic Supplementary Information (ESI) available: Computational details, wavefunction characters of excited states, frozen nuclei dynamics, character of the electronic wavefunction, time-resolved fluorescence spectra, fitting procedures of: kinetic model for intersystem crossing dynamics, fluorescence decay, and vibrational ground state recovery, average geometries of the ground and excited states in the two solvents, derivation of the proximal radial distribution function, detailed analysis of spin-orbit couplings, temporal evolution of compositions of spin-mixed states, and time-resolved spectroscopy (PDF). See DOI: 10.1039/cXCP00000x/

1 Introduction

Spin-change (intersystem crossing, ISC) dynamics is an important issue in designing photoactive transition-metal complexes. For example, ultrafast and efficient ISC is highly desirable in the case of luminophores for OLEDs or sensors, whose operation requires strong long-lived phosphorescence from the lowest triplet state, which is the case of polypyridine and phenyl-pyridine Ir^{III} complexes. On the other hand, it is a mixed blessing for light-energy harvesting, where efficient ISC wastes a significant portion of absorbed light energy but produces long-lived triplet states capable of storing a part of excitation energy through slower follow-up electron transfer processes and charge separation. Photophysics and photochemistry of heavy-metal d^6 systems is traditionally explained assuming optical excitation of metal-to-ligand charge

transfer (MLCT) or $\pi\pi^\star$ intraligand (IL) singlet excited states, from which the lowest triplet state is populated on a subpicosecond timescale with a (near) unity efficiency. Despite their very short lifetime, initially populated ^{1}MLCT states of d^6 complexes have been detected by fluorescence upconversion[1–3] and their very fast decay kinetics were customarily attributed to ISC. For example, fluorescence lifetime of were determined for complexes of Ru^{II} ($<$30 fs),[4,5] Os^{II} ($\sim$100 fs),[6] and Ir^{III} (50-110 fs).[7] It is also of relevance that UV-excited high-lying ^{1}IL excited states of Ir^{III}(2-phenyl-pyridine)$_3$ decay with a 70 fs lifetime to the lowest ^{3}MLCT state, proceeding through a cascade of steps faster than 10 fs.[8]

Rhenium(I) tricarbonyl-polypyridine complexes, which comprise another important group of photosensitizers,[9,10] show ultrafast biexponential fluorescence decay[11–13] followed by long-lived (ns-μs) phosphorescence. This is the case of the photooxidant fac-[Re(im)(CO)$_3$(phen)]$^+$ (im = imidazole, phen = 1,10-phenanthroline) whose fluorescence decays with lifetimes of 144 and 1500 fs (in N,N-dimethylformamide) that were originally attributed to a direct ISC from optically populated ^{1}MLCT to the lowest ^{3}MLCT state and to a parallel slower ISC through an intermediate ^{3}IL (phen-localized $\pi\pi^\star$ intraligand) state, respectively.[13] This picture has recently been challenged by a theoretical study[14] that simulated ultrafast excited-state dynamics of this complex employing the surface-hopping methodology[15] where the electronic wavefunction was allowed to spread over different electronic states whose nonadiabatic and spin-orbit couplings were taken into account. Solvent water molecules were included explicitly. A set of optically excited low-lying singlet states was found to undergo a $\sim$8 fs electronic-driven ISC to a 70:30 mixture of triplet and singlet states that further evolved in a nuclear-driven $\sim$420 fs "retarded" ISC, during which the overall triplet-to-singlet ratio increased only slightly to ca. 80:20 at 250 fs, while the triplet population was redistributed among various states. The population distribution at 250 fs expressed in terms of spin-free states showed significant contributions from three lowest-lying triplets and the lowest singlet, plus minor contributions from higher states. This computational result can be attributed either to a mixture of molecules in different electronic states or to a strong mixing of singlet and triplet states in the final electronic wavefunction through spin-orbit coupling. A preliminary observation of two excited-state features in IR spectra of analogous

complexes measured at 1 ps after excitation[13] supports the former interpretation. This theoretical work has very important implications for our understanding of the rich photochemistry and photophysics of Re^I carbonyl-diimine complexes and their use as photosensitizers and photocatalysts. It has showed that the conventional assignment of ultrafast fluorescence decay kinetics to ISC has to be revisited. A good match between experimental[13] and simulated[14] time-resolved fluorescence spectra suggests that femtosecond fluorescence decay kinetics has to be interpreted beyond the singlet population decay, considering the overall excited-state and structural dynamics. The intriguing possibility that a mixture of molecules in different excited states persists into the picosecond time range implies that follow-up relaxation and photochemistry can proceed through different channels.

In this work, we have focused on the prototypical member of the Re^I tricarbonyl-polypyridine family, the fac-ReCl(CO)$_3$(bpy) complex, **Rebpy**, that is well known for its 40-ns-lived phosphorescence, photoredox chemistry, and as a photo- and electro-catalyst of CO$_2$ reduction.[9,10,16] Its low-lying singlet and triplet excited states have an MLCT character but, unlike [Re(im)(CO)$_3$(phen)]$^+$, with a Cl$\rightarrow$bpy LL'CT contribution,[9,11,17–20] Similarly to [Re(im)-(CO)$_3$(phen)]$^+$, **Rebpy** fluorescence decays biexponentially with 85 and 340 fs lifetimes in acetonitrile (ACN).[11–13] It is of interest that the fluorescence decay kinetics slows down upon changing the axial ligand X in ReX(CO)$_3$(bpy) from Cl (85, 340 fs) to Br (128, 470 fs) and I (152, 1180 fs), that is opposite than expected based on increasing spin-orbit coupling.[11] This observation has led to the proposal that the ISC dynamics is governed by the Re–X stretching vibration[11] and stimulated much theoretical work, including spin-orbit and vibronic coupling calculations, as well as wavepacket propagation.[17,21–27] Photophysics and photochemistry of **Rebpy** is also affected by the solvent. Fluorescence decay slows down on going from ACN (85, 340 fs) to N,N-dimethylformamide (97, 1090 fs)[11–13] and relaxation dynamics[28–33] is solvent dependent in the 1-20 ps range. Importantly, excited-state solvation dynamics was found to determine the efficiency of **Rebpy** photoreduction by triethanolamine, which is the first step of photocatalytic CO$_2$ reduction.[34]

Excited-state dynamics that gives rise to observed biphasic subpicosecond fluorescence decay kinetics, time-dependent distribution of populated low-lying excited states, as well as the role of structural and solvation changes at early times after excitation
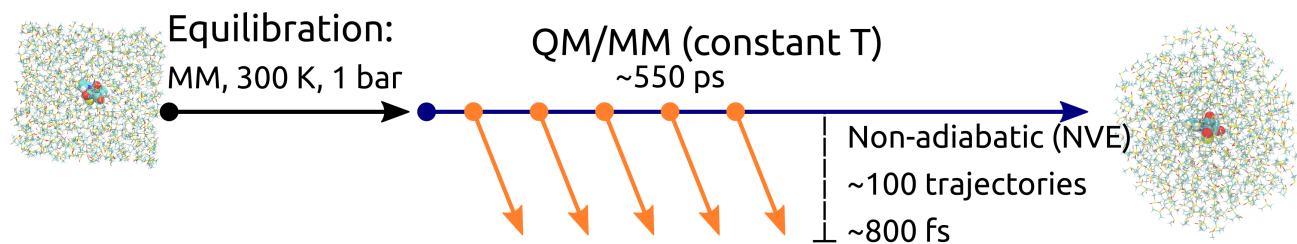
Fig. 1 Schematic description of the simulation framework of Rebpy complex in investigated solvents, illustrated for the case of DMSO. First, the simulation box was equilibrated in periodic boundary conditions using classical dynamics with a frozen Rebpy geometry (black arrow). Employing adiabatic QM/MM propagation at a constant temperature (blue arrow), initial conditions for non-adiabatic dynamics were generated . Finally, non-adiabatic dynamics simulations in an NVE ensemble were propagated (orange arrows).

are some of the photophysical questions we address in this study employing full-dimensional surface-hopping simulations. Predictions emerging from these calculations aid interpreting the fluorescence decay as well as ultrafast spectral changes and time-dependent band-shapes observed in time-resolved IR absorption (TRIR) and femtosecond stimulated Raman scattering (FSRS) spectra. The choice of solvents (Fig. S1), ACN and dimethylsulfoxide (DMSO), was motivated by distinctly different excited-state relaxation dynamics observed in our preliminary TRIR experiments. Simulations were carried out to up to 800 fs, in order to access times relevant to ultrafast excited-state reactions, such as intramolecular electron transfer.[35–38] Indeed, the present theoretical work has important implications for our mechanistic understanding of photoinduced electron transfer. For example, it is argued that (sub)picosecond photochemical processes of Re(I) tricarbonyl-diimine complexes may occur from a manifold of several excited states spread in energy, instead of being limited to the lowest triplet state only.

2 Methods

Classical simulations were performed with the Amber 14 software[39] at a constant pressure 1 bar and temperature 300 K maintained by weak-coupling thermostat and barostat, with a coupling time of 1 ps.[40] A 1 fs time step and 3D-periodic boundary conditions were employed. **Rebpy** intramolecular geometry corresponding to the ground-state energetic minimum in vacuum was fixed during classical simulations. Nonbonding interactions were determined from a generalized Amber force-field (GAFF) and partial charges were taken from a Mulliken population analysis. Solvent molecules were parametrized by the recommended protocol,[41,42] i.e., GAFF was used for bonded and nonbonded interactions, and partial charges were determined via restricted elec-

trostatic potential fitting procedure (RESP). Resulting charges for ACN and DMSO are depicted in Figure S1, ESI†.

Adiabatic QM/MM MD simulations were carried out using Amber 14 software[39] interfaced with TERAChem simulation package[43,44] employing electrostatic embedding and without periodic boundary conditions. A 1 fs time step was employed and a weak-coupling thermostat was applied.[40] Only **Rebpy** was treated quantum mechanically at a DFT level of theory: PBE0, 6-31g* basis for non-metallic atoms, LANL2DZ basis for Re with effective core potential[45] and D3 dispersion correction.[46,47] Solvent was described at a MM level with the same parameterization as in classical simulations.

Non-adiabatic QM/MM MD simulations were performed in a fewest-switches surface hopping[48] fashion employing the SHARC package[49] interfaced with ORCA and Tinker.[50] QM/MM MD calculations employed PBE0 functional, ZORA relativistic Hamiltonian,[51] ZORA-def2-SVP[52] basis set for non-metallic atoms, SARC-ZORA-TZVP[53] basis set for Re, D3 dispersion correction[46,47] and SARC/J auxiliary basis set.[54] The system was propagated at a constant energy (i.e., in a microcanonical ensemble) with a 0.5 fs time step. In the non-adiabatic framework, the energy based decoherence[55] was used, non-adiabatic coupling vectors were replaced by wavefunction overlaps[56] and the time step for three-step wavefunction propagator[57] was of 0.005 fs was used. Surface hopping was performed on diagonal (spin-mixed) surfaces.

Preparation of initial conditions is schematically described in Figure 1. A cubic box with dimensions $40 \times 40 \times 40\,\text{Å}$ containing **Rebpy** and 550 DMSO molecules was created. The simulation box was then equilibrated at a constant temperature (300 K) and pressure (1 bar) employing 3D-periodic boundary conditions, geometry of **Rebpy** was frozen during this step. The equilibration step was followed by several long QM/MM simulations (of to-

tal length 550 ps) starting from different points of the MM/MD equilibration run at a constant temperature and without periodic boundary conditions. 500 snapshots with temporal spacing of 1 ps were extracted from the generated trajectories and served as initial conditions. Vertical excitations considering 20 singlet and 20 triplet states were performed for each initial condition in order to determine the initial active state.[14] Out of these, 100 initial conditions were selected and simulated in non-adiabatic dynamics. Non-adiabatic trajectories were simulated for up to 800 fs. 8 trajectories started in S_1 state, 92 in S_2.

The simulation set in ACN was prepared in a similar manner to DMSO. A cubic box with dimensions $40 \times 40 \times 40$ Å containing **Rebpy** and 950 ACN molecules was created. The simulation box was then equilibrated at a constant temperature (300 K) and pressure (1 bar) employing 3D-periodic boundary conditions, with the **Rebpy** geometry frozen during this step. The equilibration run was elongated to a nanosecond time scale. Next, 500 uncorrelated snapshots were generated for further prolongation as QM/MM trajectories at a constant temperature and without periodic boundaries up to 2 ps. For each of resulting 500 initial conditions a vertical excitation with 20 singlet and 20 triplet state was computed and the initial active state determined. In this case, 97 non-adiabatic trajectories were simulated for up to 770 fs, from which 4 started in S_1 state and 93 in S_2.

3   Results and Discussion

Non-adiabatic TD-DFT (Time-Dependent Density Functional Theory) molecular dynamics simulations of electronically excited **Rebpy** were carried out in two different solvents (ACN, DMSO) on spin-mixed potential energy surfaces,[57] as implemented in the SHARC package (Section S.1 in ESI†).[49] The electronic ground state is labeled as GS, excited singlet states as $S_1, S_2, S_3, \ldots, S_n$ and excited triplet states as $T_1, T_2, T_3, \ldots, T_n$. The choice of the initial active state for non-adiabatic dynamics was based on analysis of **Rebpy** electronic absorption spectrum (Figure 2) calculated from a large number of initial conditions (uncorrelated positions and velocities). Excitations were simulated with an infinitely narrow pulse, hence only transition between states with the same multiplicity as the ground state, i.e., singlets, are relevant at time zero. After vertical excitation to the singlet manifold at time zero, 97 non-adiabatic trajectories (4 starting in S_1 and 93 in S_2) were simulated for 770 fs in ACN and 100 non-adiabatic trajectories

(8 starting in S_1 and 92 in S_2) were simulated for 800 fs in DMSO.

Figure 2 compares calculated and experimental electronic spectra of **Rebpy** in the UV-Vis region. The computed spectrum in ACN reproduces the shape of the experimental spectrum, with the lowest-energy feature red-shifted with respect to the experiment.

In agreement with previously published results,[11–13,59–61] the two lowest singlet and triplet states have $Re(CO)_3 \rightarrow$ bpy MLCT character with ca 20% Cl $\rightarrow$ bpy LLCT admixture (Figure S3, ESI†). The solvation environment affects the character of the electronic wavefunction only slightly. It is supposed that the S_2 state will be preferably populated by excitation in the visible region, and then undergoes ISC to lower energy states T_2 and T_1. The rightmost plot in Figure 2 depicts the experimentally used laser pulse energies (3.1–3.25 eV).[11,13,58] In order to populate experimentally relevant active states, the energy window for excitations (2.7–3.0 eV) was used in the calculations. This ensures that sufficient number of initial conditions for non-adiabatic trajectories will be produced. Characters and densities of states at time zero are discussed in detail in the Section S.2 in ESI†.

3.1   Intersystem crossing

Figure 3 presents the temporal evolution of four predominantly populated spin-mixed states for simulations in both solvents (left), together with their compositions (right). In both solvents, the MLCT and LLCT characters of the lowest singlet and triplet individual spin-free states are preserved during the whole simulation time (full plots are showed in Section S.4 in ESI†).

At the beginning of simulations, the wavefunction is described predominantly by State 9 (red line). This state is bright and contributes significantly to the fluorescence.[12,13,17] During the simulation, the contribution of State 9 diminishes continuously to ca 15 % at 800 fs. After laser-pulse excitation in ACN the population of State 8 (blue) rapidly increases in the first 350 fs, followed by a slow gradual increase, reaching ca 40 % at 770 fs. In contrast, the population of State 8 in DMSO reaches a maximum at about 500 fs and then decreases to ca 30 % at 800 fs. The contribution of State 4 (green line) grows continuously to ca 30 % in both solvents. At around 500 fs the differences in contributions of spin-mixed states between the two solvents becomes apparent. The most prominent changes concern States 9 and 8. At long times the ensemble of molecules can be still described by spin-mixed states which most likely evolve toward an equilibrium that
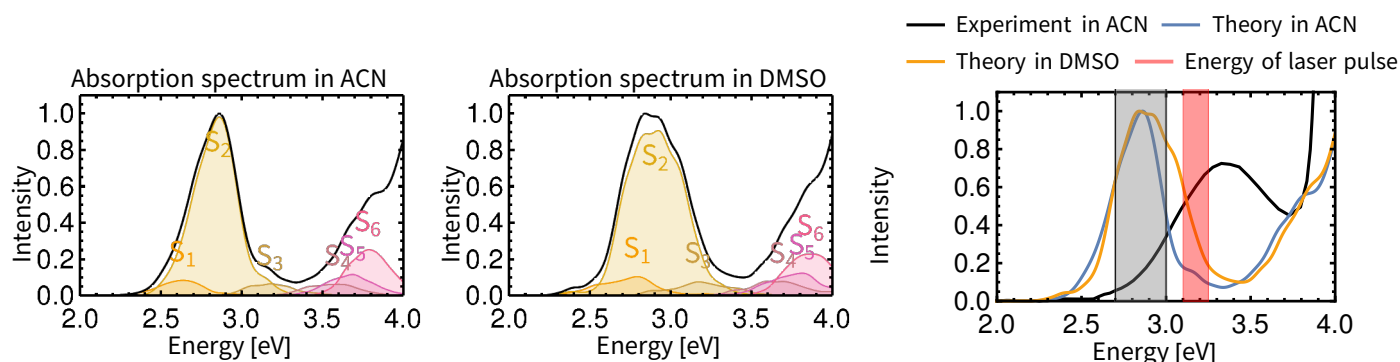
Fig. 2 TD-DFT calculated electronic absorption spectra of Rebpy in ACN (left) and DMSO (right). The final spectrum is represented by a solid black line, contributions of the six lowest-lying singlet states are given in colour. The rightmost panel compares simulated and experimental spectra in ACN. The red window depicts the laser-pulse energy used in most photophysical experiments.[11,13,58] The gray shaded area shows the energy window used for excitation in this work.
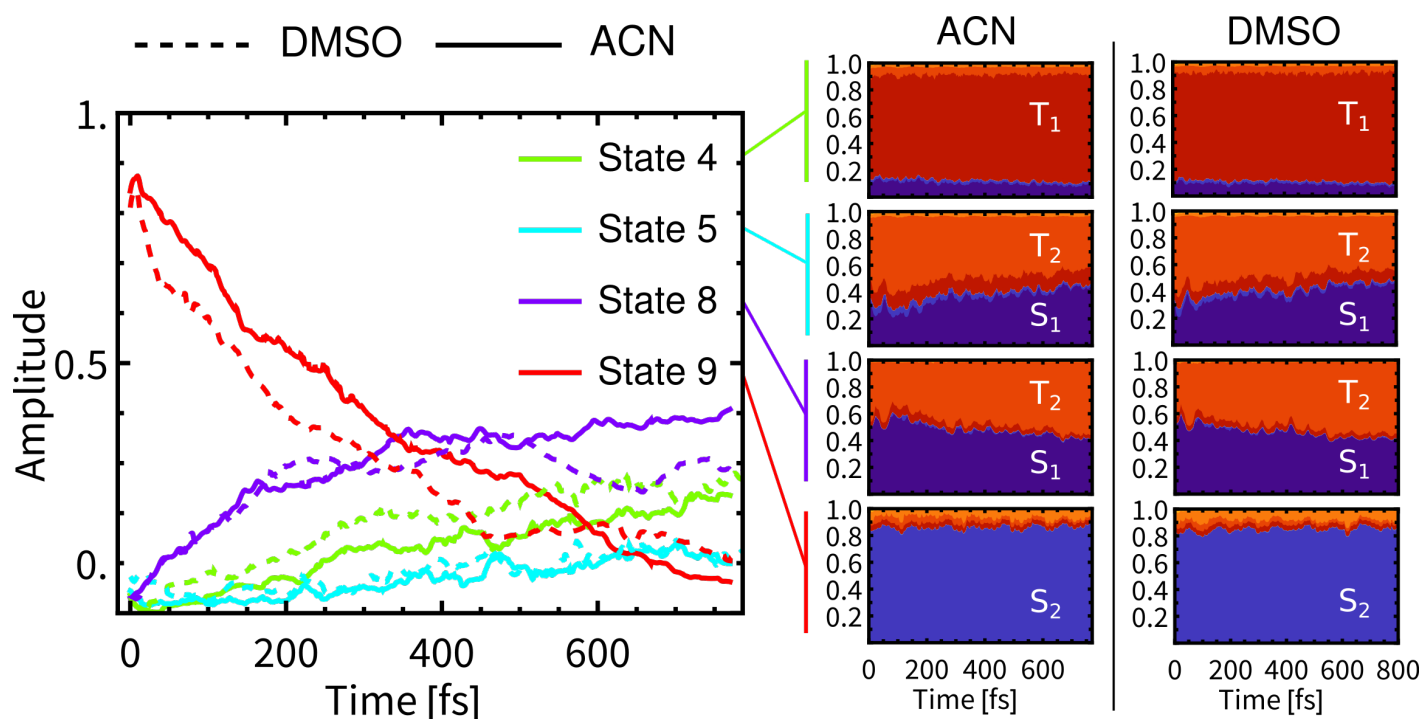

Fig. 3 Left: Development of populations of spin-mixed states (left panel) in DMSO (dashed) and ACN (full). Only four most populated states are plotted (State 1 is the ground state). Right: Composition of spin-mixed states in a spin-free basis. The spin-free representation was obtained via ensemble averaged columns of transformation matrix $\mathbf{U}$ defined in Ref.[57]. The evolution of all spin-mixed states is presented in Figure S15, ESI†. Compositions of the lowest 20 spin-mixed states represented in Figures S16, S17, ESI†.

could persist in the ps timescale. Such behavior can explain an observed formation of additional band in time-resolved infrared spectra (Section 2.6).

The average composition of spin-mixed states varies only slightly during simulations in both solvents (Figure 3-right). State 9 remains predominantly composed of the S_2 state and thus will have a significant contribution to the fluorescence. Luminescence from State 8 is expected to be weak since S_1 exhibits only a small transition dipole moment to the ground electronic state,[17] moreover

the contribution of S_1 decreases over the simulation time being compensated by a raising contribution of T_2. Experimentally observed long-lived phosphorescence on ps timescales[11] can be assigned to States 8 and 4, since their populations persist to longer times and they have a significant contribution of S_1. State 4 is mainly composed of T_1 and, along with States 2 and 3 (also mostly T_1), it will be the final state after the ISC. However, these states will become predominant at much longer times than the total simulation time.
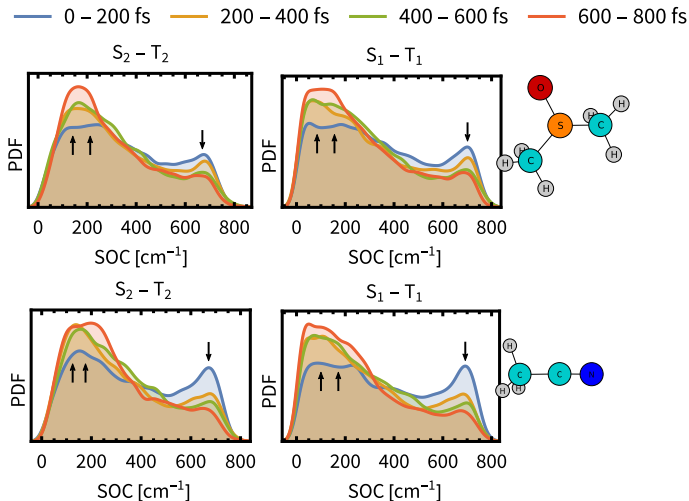
As above analysis may have lost some information about the composition of spin-mixed states by ensemble averaging, we have analysed individual spin-orbit coupling matrix elements (SOCMEs) and inspected the temporal evolution of their distribution (Figure 4). As a common trend for both solvents we found a minor increase of S_1–T_2 and S_2–T_1 couplings, and a more significant decrease of S_1–T_1 and S_2–T_2 couplings. The observed decrease of S_1–T_1 and S_2–T_2 SOCME in ACN is faster than its counterpart in DMSO, which may lead to a decreasing rate of the ISC (slow component τ_{slow}).

3.1.1 Time-evolution of singlet and triplet populations.

The description of the ensemble of Rebpy molecules in terms of time-dependent populations of spin-mixed states (Figure 3) can be transformed into spin-free representation,[57] which is chemically more intuitive, and related to the notion of intersystem crossing (Figure 5). While the temporal evolution of ensemble-averaged singlet and triplet electronic populations in both solvents is shown in the left panel, the right panel displays biexponential kinetic fits, characterized by time constants τ_{fast} and τ_{slow}. At time zero, only singlet states were populated due to a δ-pulse excitation.[14] On the timescale of τ_{fast} (up to 6 fs) ca 20 % of singlet population was converted to triplets. τ_{fast} is attributed to the temporal evolution of the molecular spin-orbit wave packet introduced by Mai and González.[14] By employing the frozen-nuclei dynamics[14] (Section S.3 in ESI†), we proved that this initial con-

version is a purely electronic effect, independent of non-adiabatic effects, which operates on a few-femtosecond timescale. Estimated τ_{fast} values are comparable to that of the $[Re(CO)_3(im)(phen)]^+$ complex,[14] in which, however, the initial singlet to triplet conversion yield is about 70 %.

After relaxation of the molecular spin-orbit wave packet a minor decrease of triplet population in 10-100 fs was observed in ACN and is mirrored by an increase of the singlet population. As would be expected after the formation of the quantum wave packet at time zero, due to the interaction with the environment the wavefunction of the system will eventually collapse into one electronic state. Apparently, the spin-orbit electronic state with the major contribution to the wavefunction is dominated by singlet states, hence the increase of singlet population. This effect is, however, quickly superimposed by non-adiabatic effects, that lead to increasing population of triplet states.

Biexponential global fits of time-dependent total singlet and triplet populations provided time constants τ_{slow} of approx. 1000 fs and 800 fs were obtained for DMSO and ACN, respectively. The time constant τ_{slow} is attributable to the intramolecular vibrational redistribution (IVR) with frequent non-adiabatic effects that drive further singlet-to-triplet conversion and population redistribution within the singlet and triplet manifolds (Figure 5, left). It follows that non-negligible singlet population persists on longer simulation times, which is attributed to reaching an equilibrium between spin-mixed electronic states but also to a minor admixture of singlet states to final electronic states through the spin-orbit interaction. The "slow" ISC component is slightly slower in DMSO ($\sim$1000 fs) than in ACN ($\sim$800 fs). The evolution of the ensemble-averaged excited-state characters is virtually identical in both solvents, with only minor differences in the first 100 fs (Section S.4 and Figure S5 in ESI†).

A comparison of **Rebpy** (τ_{fast} 1-6 fs, 20 %; τ_{slow} 800-1000 fs) with $[Re(CO)_3(im)(phen)]^+$ (τ_{fast}=8 fs, 70 %; τ_{slow}=420 fs, Ref.[14]) indicates large effects of the coordination sphere composition and excited-state character on ISC kinetics and yields. Namely, the majority of singlet states in $[Re(CO)_3(im)(phen)]^+$ is converted during the fast wave packet relaxation, in contrast with **Rebpy** where most of ISC appears to be IVR-driven, occurring in the "slow" kinetics component. In both cases, the "slow" kinetics converts only units of percent of the singlet population per 100 fs (Figure 5). This difference can be attributed to the lack of low
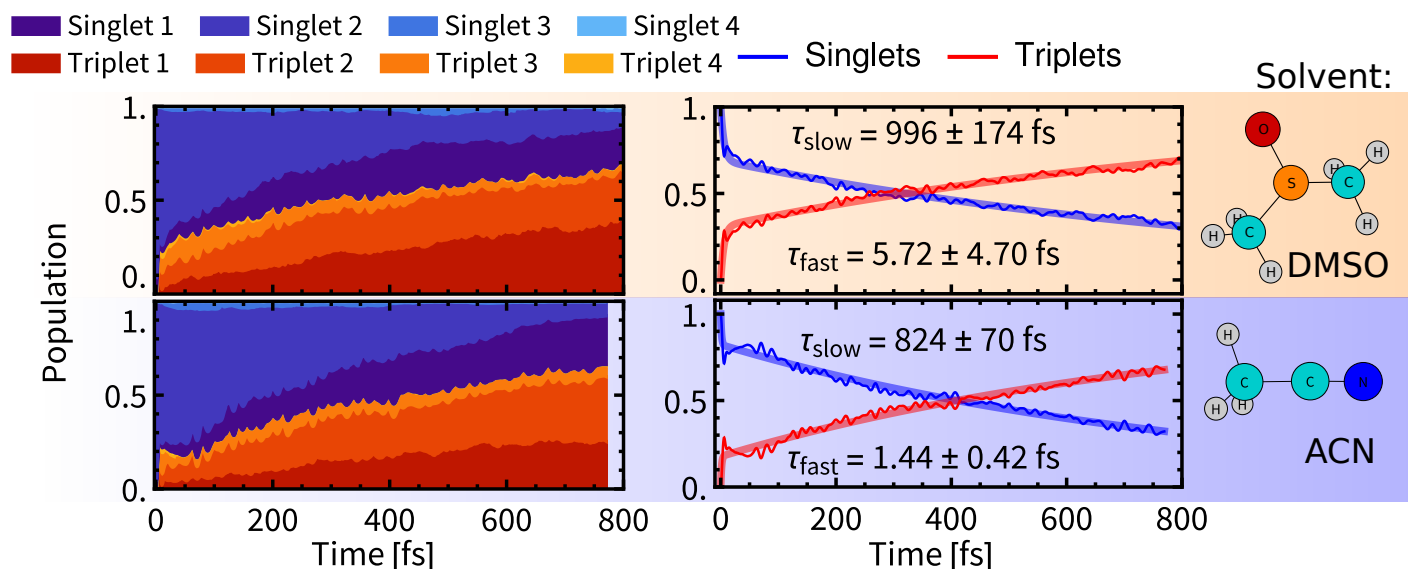
Fig. 5 Left: temporal evolution of singlet and triplet spin-free states. Right: temporal evolution of total singlet and total triplet populations fitted with bi-exponential kinetics. Details of the fitting procedures can be found in Section S.6, ESI†.

frequency Re-Cl vibration in the imidazole complex and different excited-state characters as a bright state of $[\text{Re(CO)}_3(\text{im})(\text{phen})]^+$ lacks the LL' contribution and MLCT amounts to ca 70 %.

3.2 Luminescence decay

Experimental time-resolved luminescence spectra (Figure 6-right) obtained upon 80 fs, 400 nm excitation exhibited a very broad band peaking at about 530 nm that has rapidly decayed in intensity and shifted to the red, eventually converting into a long-lived weak phosphorescence signal at ≈610 nm. The initial decay kinetics is biexponential. The time constants $\tau_1 = 85$ fs and $\tau_2 = 340$ fs were determined in ACN and attributed to the direct ISC from the optically prepared ^{1}MLCT S_2 state to T_1 and to an indirect process via an intermediate triplet state, respectively. [11,12] To understand the apparent contradiction with the simulated ISC dynamics, we have simulated also the time-resolved luminescence spectra, assuming that the emission intensity is proportional to the total singlet population times the transition moment that was calculated explicitly at each time delay. Calculated radiative transitions were broadened in time by a 100 fs full width at half maximum (fwhm) Gaussian to mimic the experimental response function and also in the energy domain by a 0.5 eV fwhm Gaussian to obtain continuous spectral bands (Section S.5, ESI†). Simulated luminescence spectra and decay kinetics show a good match with the experiment (Figures 6, 7). Fitting parameters $\tau_1 = 72$ fs and $\tau_2 = 343$ fs of our simulation results are in an excellent agree-

ment with the global kinetic fit of experimentally measured time-resolved fluorescence spectra in ACN. [11]

A comparison of luminiscence decay kinetics in the two solvents reveals that the time constants τ_1 are similar, i.e., about 70 fs, being consistent with the experimental finding that τ_1 depends only slightly on the quality of the solvent. [12] On the other hand, τ_2 possesses some solvent-specificity with a slightly faster luminescence decay in ACN, $\tau_2 = 343$ fs than in DMSO, $\tau_2 = 388$ fs.

Importantly, the luminescence decay lifetimes τ_1 and τ_2 are substantially different from the τ_{fast} and τ_{slow} lifetimes of the singlet-population decay (Figure 5). This indicates that fluorescence decay cannot be solely driven by the ISC and that ultrafast time-evolution of luminescence spectra does not originate solely from changing populations of emitting states. A changing value of the transition moment and, presumably, population redistribution within the singlet-state manifold in the course of the IVR and structural relaxation appear to be important factors in the present case. Changing interactions with the solvent environment will influence the luminescence as well.

Comparable rates of the ISC in both solvents and faster decay of the luminescence decay component (τ_2) in ACN along with good agreement with experimental data give raise to an important question: *What quantity is actually affected by a presence of explicit solvent molecules*? Due to similar dielectric constants, the faster luminescence decay may originate from direct interactions of **Rebpy** with explicit solvent molecules. In the next sections we
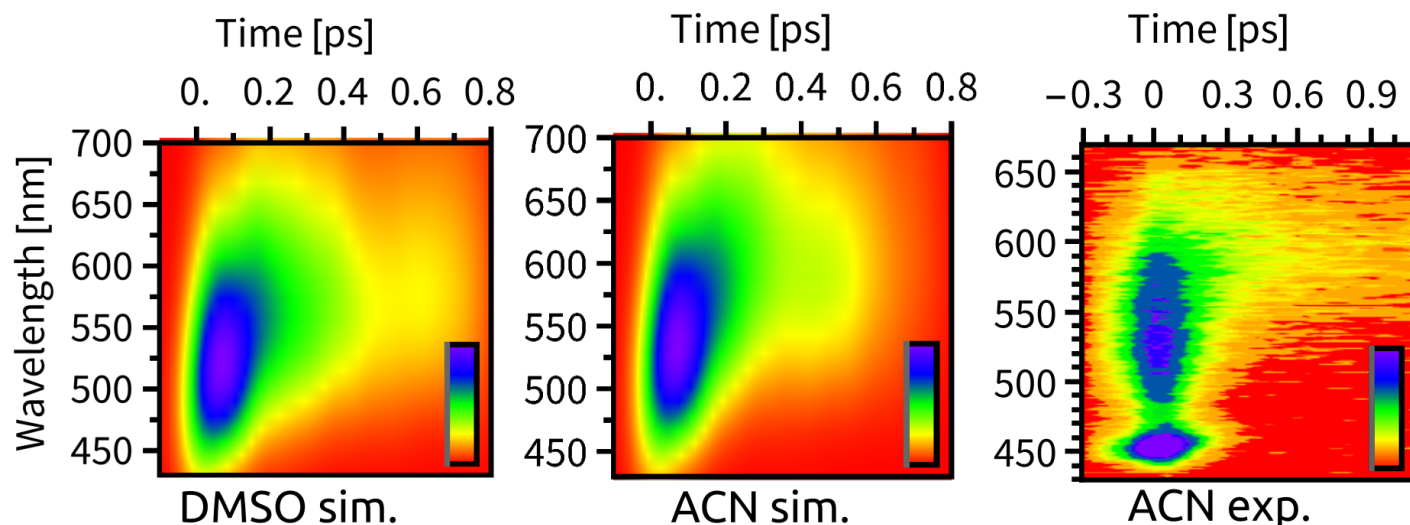
Fig. 6 Time-resolved fluorescence spectra, from left to right: simulated spectrum in DMSO, simulated spectrum in ACN, experimental spectrum in ACN from Ref.[11].We note that the peak at ∼450 nm in the experimental spectrum is the ACN Raman line.
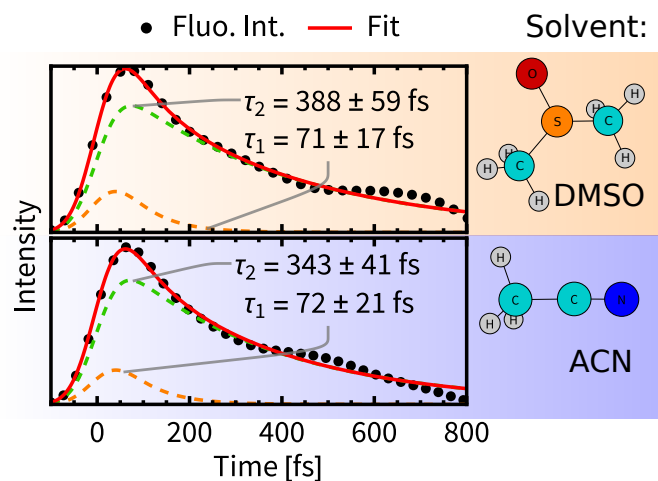

Fig. 7 Decay of total fluorescence intensity convoluted with the instrumental response function (dots) fitted with bi-exponential decay (red line). For details of the fitting procedures see Section S.6, ESI†.

will examine which quantities could be affected by such specific solvation.

3.3 Structural relaxation dynamics

As a measure of structural changes of **Rebpy** during the ISC we used the time evolution of the root-mean-square deviation (RMSD) from the geometry at time zero. Results shown in the right panel of Figure 8 represent the ensemble average over all trajectories, allowing to follow a net evolution (deviation) of **Rebpy** geometry. The temporal evolution of RMSD follows exponential kinetics, but the interpretation of fitted time constant is not straightforward. On physical grounds, we may interpret τ_{RMSD} as a rate of motion in the space of geometries. That is a rate of motion

from the ground electronic state region to the region of excited states. In order to get a better insight into this *geometric relaxation*, time evolution of geometry ensembles was monitored by means of cluster analysis (Figure 8-left). To that end, two references, the average geometry of the main GS cluster (about 70 % of all frames) and the average geometry of the near-equilibrium excited-state cluster (i.e., simulation time window 650–800 fs, about 70 % of frames) were defined. Next, for different time windows, geometries of **Rebpy** in the main cluster (about 70 % of all frames) were characterized by their distance (measured as RMSD) to these two references.

Results from the clustering analysis (Figure 8-left) offer an intuitive interpretation of the geometric relaxation. In the electronic GS, **Rebpy** geometries exhibit a narrow distribution with a low mean value in the $RMSD_{GS}$ domain (black curve), i.e., they are close to the average GS geometry. In the first 100 fs (red and purple curves) the distribution of **Rebpy** geometries evolves towards the diagonal which results in a broad distribution of RMSD with respect to both GS and near-equilibrium excited state. In time windows 100–150 fs and 150–200 fs (blue and green curves) the distribution gets bellow the diagonal, i.e., $RMSD_{Ex}$ decreases and narrows, while $RMSD_{GS}$ grows and broadens.

Only minor changes in distribution are observed beyond 200 fs, meaning that **Rebpy** geometries are fluctuating around the new equilibrium. The actual transition from the average GS geometry to that of near-equilibrated excited state is described by alignment of bpy and equatorial CO ligands into a single plane (see
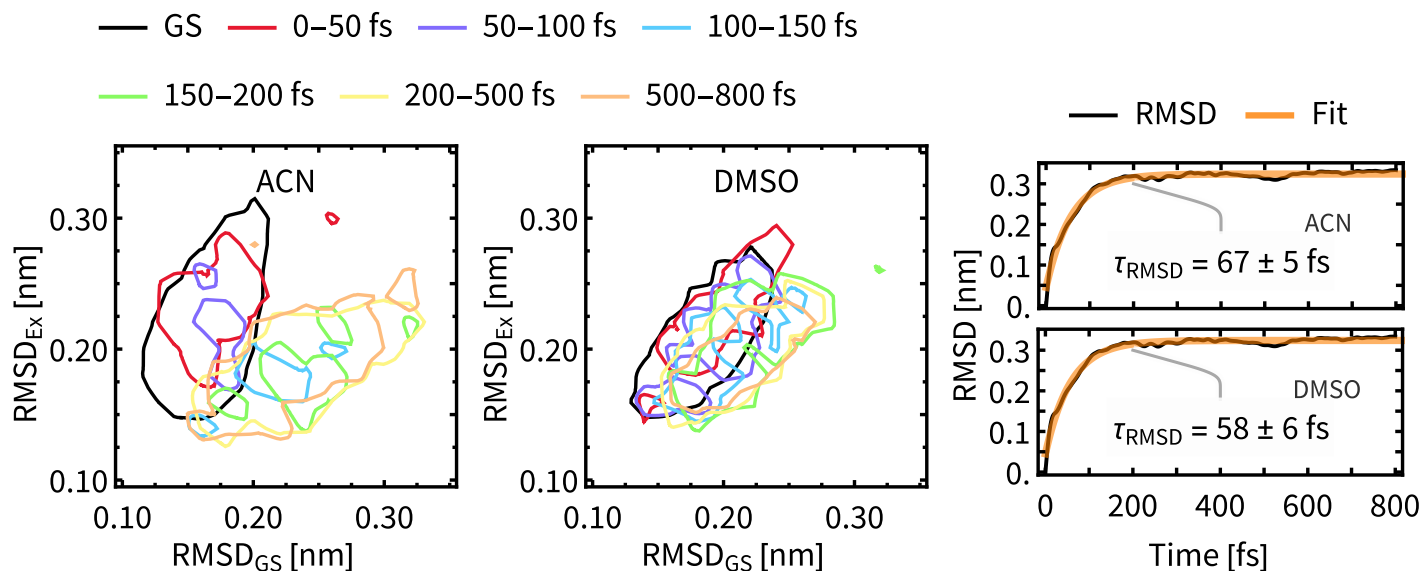
Fig. 8 Left panels: Temporal evolution of the 2D-distribution (at 50% contour level) of the main cluster of the ensemble of geometries, evolving from the initial GS (black line) towards new equilibrium state (see the legend for color coding). The x-axis measures the RMSD to the average geometry of the main GS cluster. The y-axis measures the RMSD to the average geometry of the main cluster of simulation time 650–800 fs, which should be close to the new equilibrium state. Right panel: Temporal evolution of the average RMSD from the GS structure in the two solvents fitted with an exponential function. Temporal evolution of RMSD was computed for each trajectory and averaged afterwards.

Figure S9, ESI†). In both solvents the geometric relaxation is significant only in first 200 fs, distributions of geometries in ACN are, however, much broader than in DMSO. This indicates a more compact and stiffer **Rebpy** geometry ensemble in DMSO. Also, geometric relaxation is faster in DMSO since the distance from the GS region to the near-equilibrium excited state region is on average shorter than in ACN.

The time constants for geometric relaxation $\tau_{\mathrm{RMSD}}(\mathrm{ACN}) = 67$ fs and $\tau_{\mathrm{RMSD}}(\mathrm{DMSO}) = 58$ fs are close to the time constants calculated for luminescence decay $\tau_1(\mathrm{ACN}) = 72$ fs and $\tau_1(\mathrm{DMSO}) = 71$ fs. We propose a close connection between τ_{RMSD} and τ_1, the luminescence decay at short times is driven by bleaching of the oscillator strengths due to the structural relaxation of **Rebpy**. The closer connection between structural relaxation and luminescence decay kinetics is established in Figure 9 where a strong anti-correlation is observed on simulation times 10~200 fs.

The faster luminescence decay component τ_1 thus appears to be driven by geometric relaxation of **Rebpy**. It is, however, not possible to completely disentangle the contribution of ISC to the time constant τ_1, because of its non-negligible impact on the oscillator strengths. In another words, the active electronic state determines the **Rebpy** geometries (and specific solvation), but also the actual **Rebpy** geometry (and specific solvation) steps in the selection of the active electronic state. Another implication of these
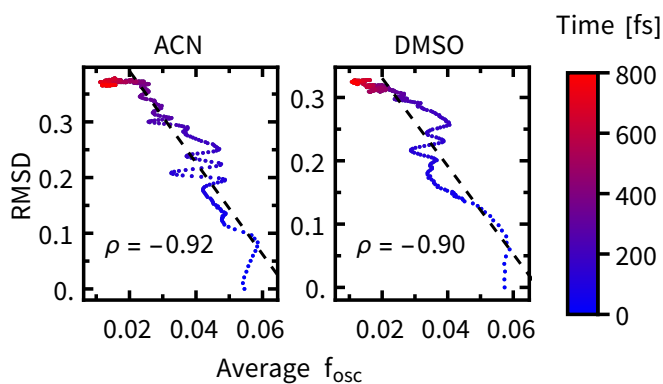

Fig. 9 RMSD plotted against the average oscillator strength at different times after excitation (color-coded), ρ represents the correlation coefficient over the 0–200 fs interval (black dashed line).

findings is that at short times (<200 fs) the overall change of total luminescence is not directly proportional to the population of any electronic state, which limits applicability of time-resolved fluorescence spectroscopy in determining kinetics of ultrafast photochemical and photophysical processes.[11–13]

3.4 Solvent relaxation dynamics

On simulation times above 200 fs, the structural relaxation of **Rebpy** is no longer an important process whereas relaxation of the solvent environment persists. Solvent dependence of the calculated (Figure 6) as well as experimental[11–13] time constant τ_2 (Figure 7) could be explained by different relaxation of solva-

tion shells around **Rebpy**. As a measure of solvent relaxation, we employed the proximal radial distribution function[62,63] (pRDF, described in Section S.8, ESI†), which allowed us to monitor solvation in the vicinity of each ligand within **Rebpy**.

In Figure 10, we present non-equilibrium solvent distribution during non-adiabatic dynamics with temporal resolution of either 100 or 200 fs. Equilibrium distributions in the ground electronic state (GS) and in the lowest triplet state (denoted as T_1 – limit) are serving as references to estimate the solvent relaxation kinetics.
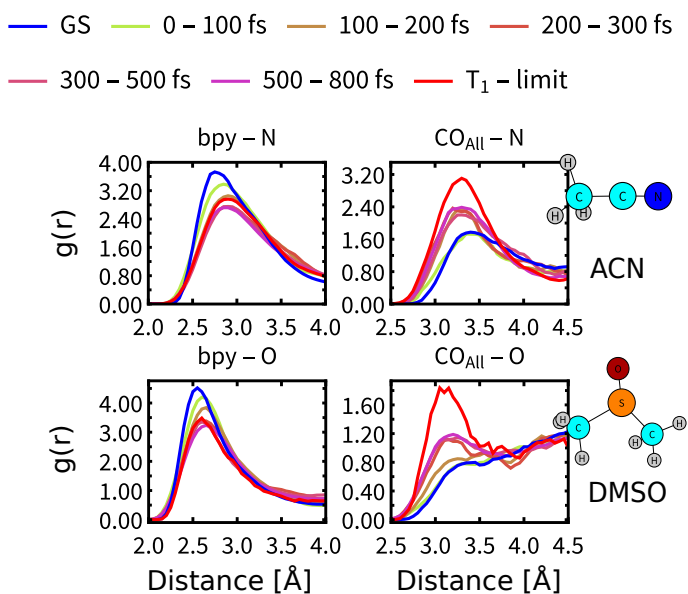

Fig. 10 Proximal radial distribution functions of negatively charged solvent atoms (O in DMSO, N in ACN) to the bipyridine ligand and all carbonyl ligands. Blue lines represent distribution in the ground electronic state, red lines the limiting distribution in fully relaxed lowest triplet state (T_1, computed from Born–Oppenheimer dynamics for times 5–10 ps). Colours denote different time intervals during nonadiabatic simulations.

The solvation shell around a bipyridine ligand experiences a decrease of the density of negatively charged solvent atoms (O, N) after excitation, which can be explained by decreasing charge on the bipyridine ligand due to an $Re(CO)_3 \rightarrow$ bpy MLCT character of the populated excited states. On the contrary, the solvation shell in the vicinity of carbonyl ligand experience increasing density of negatively charged solvent atoms caused by electron density transfer from carbonyls (becoming more positively charged) to bipyridine.

pRDFs describe relaxation as an increase (enrichment) or decrease (depletion) of the local density of negatively charged atoms in the first solvation shell, which cannot be viewed as a complete

solvent reorganization. We can make a use of an experimental study by Horng *et al.*,[64] based on measuring a solvent response to a sudden change of electrical field and determined dielectric relaxation times of 150 fs for ACN and 900 fs for DMSO, thus predicting faster relaxation of ACN by a factor of six. We note, that experimental measurements of **Rebpy** in polar solvents and our theoretical approach resembles a principal similarities with above mentioned study. Quantitative agreement is, however, not expected, since in the Ref.[64] the solvent relaxation was studied around a planar molecule (Coumarin 153) while the **Rebpy** complex has a substantial 3-dimensional structure.

Comparison of the pRDF evolution from the GS distribution towards the T_1 – limit stresses much faster relaxation of ACN than DMSO molecules. It takes less than 200 fs for ACN molecules to approach the new equilibrium distribution around bpy, whereas DMSO molecules need almost 300 fs. Situation around carbonyl ligands is qualitatively different, relaxation of DMSO is again slower by approximately 100 fs but system is approaching a different equilibrium distribution than that of the T_1 state (see right panels of Figure 10). This is a clear indication that relaxation of the solvent environment is also not a single-step process and will differ for each site of **Rebpy**. The limit distribution of T_1 state around carbonyl ligands will be reached at times well beyond the total simulation time.

In summary, after approximately 200 fs only two relaxation processes are persisting: i) The ISC driven by substantial nonadiabatic effects occurring during the whole simulation times. This process has a similar rate in both ACN and DMSO solvents. ii) Relaxation of the solvation shell, whose rate is different for each solvent. iii) Decay of the total luminescence that was on a shorter time scale driven by geometric relaxation and independent of the solvation environment as was described in the previous section and experimental studies.[12] At longer times it is the relaxation of solvent environment what drives the rate of the luminescence decay. Another major cause of decaying luminescence is the ISC which, however, cannot alone explain the different behaviour in ACN and DMSO since the ISC rates are comparable in both solvents.

3.5 Coherent vibrational motions – vibrational ground state recovery

Excitation of a molecule with the δ-pulse (or generally with a femtosecond laser pulse) will in many cases form a vibrational wave packet motion.[65–67] Although surface hopping dynamics do not allow for existence of discrete vibrational levels, a coherent motion of atomic nuclei in the ensemble of trajectories is allowed and resembles the motion of the vibrational wave packet.[67] Such classical coherent motion is initiated at time zero by excitation from the ground electronic state to the excited state and dephased over time by intra- and intermolecular perturbations.[67] In our case, intramolecular perturbations are represented by changes of electronic states, and intermolecular perturbations by the solvent motion.

In order to find coherent motions, the simulated non-adiabatic trajectories were transformed from Cartesian to normal coordinates and averaged. Visual inspection then uncovered significant oscillations of the average values for four normal modes, indicating their coherent motion in the ensemble of trajectories. Global fitting with damped sine functions then determined the dephasing time constant $\tau_{\text{Deph.}}$ for each solvent. The function for global fitting of oscillating average values of normal coordinates Q_i has the form:

$$Q_i = A_i \sin\left(2\pi \cdot f_i \cdot t + \phi_i\right) \cdot \exp\left(-\frac{t}{\tau_{\text{Deph.}}}\right) + b_i \qquad (1)$$

where values with subscript i are specific for each normal coordinate, namely: A_i is the amplitude, f_i is the frequency of the vibration, ϕ_i is the phase shift, and b_i is the new equilibrium value of the normal coordinate. Importantly, the time constant $\tau_{\text{Deph.}}$ is assumed to be universal for all normal coordinates and captures the dephasing of the coherent motion.

Most significant oscillations were identified for four normal modes, which are depicted in Figure 11. All of them are low in the frequency range (200–500 cm^{-1}) and dephase with $\tau_{\text{Deph.}}$ of ca 1 ps in both solvents. This indicates a long-lived vibrational wave packet that could persist into the ps time scale. The experimental confirmation could be, in principle, given by extreme-ultraviolet transient absorption spectroscopy.[68,69] Such method would, however, require a substitution of Cl ligand for I in order to observe the excitations from $4d$ orbital at iodine site.

We can assume that intramolecular perturbations are simi-

lar for each solvent, since the ISC rates are comparable. Intermolecular perturbations are, however, different because of different solvation rates of ACN and DMSO. The similarity of the dephasing time constants for ACN ($\tau_{\text{Deph.}} = 1147$ fs) and DMSO ($\tau_{\text{Deph.}} = 1023$ fs) indicates that intramolecular perturbations (i.e., changes of the electronic states) dominate the dephasing of the vibrational wavepacket. Moreover, the time constants for the "slow" ISC component, τ_{slow}, which are a direct measure for the intramolecular perturbations, are close to the $\tau_{\text{Deph.}}$.

3.6 Nonadiabatic dynamics effects in time-resolved vibrational spectroscopy

Some of the predictions of our nonadiabatic dynamics simulations have important implications for interpreting experimentally measured time-resolved spectroscopic data and ultrafast photochemical reactivity. Whereas the sub-10 fs ISC is experimentally largely elusive, the IVR- and solvation-driven "slow" ISC, and the simultaneous presence of molecules in different electronically excited states persisting into times longer than 800 fs (Figures 3, 5) can be tested experimentally. Time-resolved vibrational spectroscopy is especially suitable since time-resolved IR absorption (TRIR) and femtosecond stimulated Raman scattering (FSRS) provide complementary insights into **Rebpy** excited-state dynamics by monitoring C≡O stretching vibrations, $\nu(\text{C}≡\text{O})$, of the Re(CO)$_3$ fragment and bpy-ligand vibrations, respectively. Our previous FSRS study[70] of **Rebpy** in ACN and ACN-d3 have shown an evolving excited-state feature with 4-5 apparent maxima in the 1475–1600 cm^{-1} range, which coalesce into two bands at about 200 fs. Its total intensity grows with time constants of 380 fs and 21 ps. Finally, it evolves into two distinct bands at 1500 and 1546 cm^{-1} due to interring $\nu(\text{C–C})$ and aromatic $\nu(\text{CC})/(\text{CN})$ vibrations of the relaxed excited state, respectively (Figure S18, ESI†). In view of the present simulations, the initial band-shape changes likely reflect the changing molecular geometry (Figure 5) and the 380 fs rise component is attributable to IVR/intramolecular restructuring and can be qualitatively related to the "slow" ISC process.

IR spectra of Re(I) tricarbonyl-polypyridine complexes show strong $\nu(\text{C}=\text{O})$ bands that shift to higher wavenumbers upon MLCT excitation, owing to diminishing Re→O π back-donation.[71–75] The behavior of the highest $\nu(\text{C}≡\text{O})$ band due to the in-phase totally symmetrical stretching vibration of the three C≡O ligands (labeled A'(1))[71] is especially informative (Figure 12). The excited-
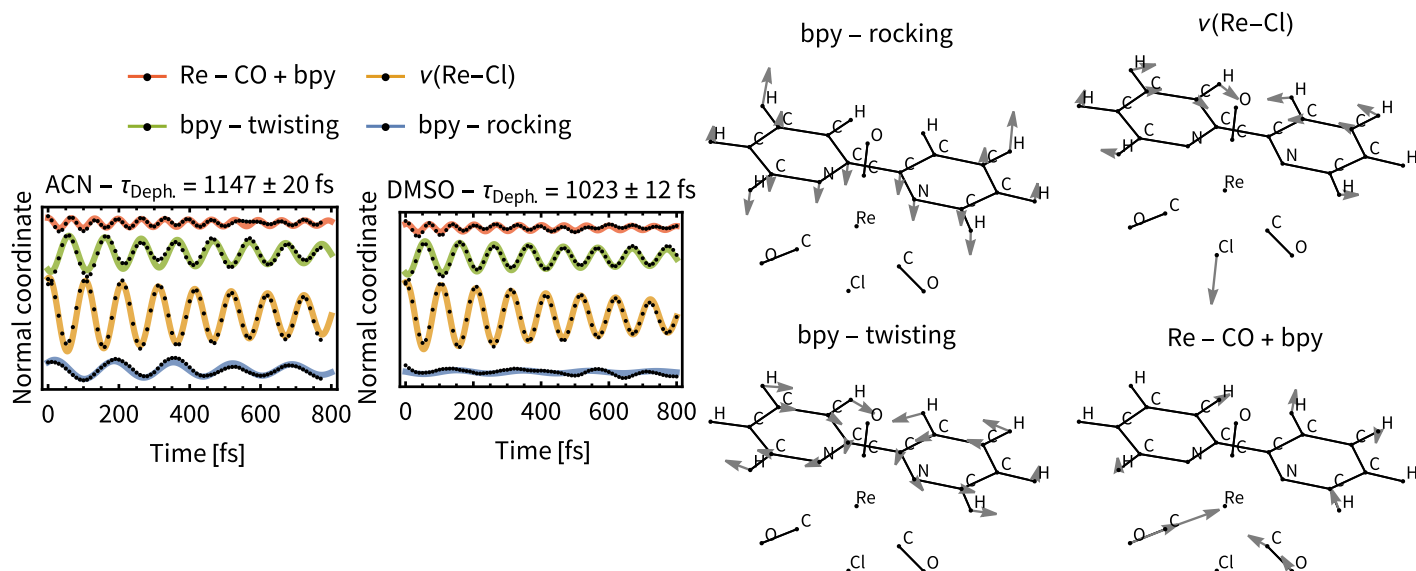
Fig. 11 Left: Oscillations in the ensemble average value of important normal coordinates (black points) and fitted damped sine functions (colour lines). Coherence dephasing times were obtained by global fitting. Right: Relevant normal modes of Rebpy, their harmonic frequencies are: $209\,\text{cm}^{-1}$ (bpy − rocking), $256\,\text{cm}^{-1}$ (v(Re–Cl)), $271\,\text{cm}^{-1}$ (bpy − twisting) and $434\,\text{cm}^{-1}$ (Re–CO + bpy).

state A′(1) band emerges concomitantly with laser-pulse excitation as a broad unresolved asymmetric feature that envelops several close-lying IR bands. It rapidly (fs-ps) shifts to higher wavenumbers and narrows, gradually acquiring a shape of an asymmetric band that can be fitted by two Gaussian peaks – one coinciding with the spectral band maximum and a minor peak that accounts for the low-wavenumber tail. The most dramatic bandshape changes occur within the first 4 ps after excitation. The composed character of the excited-state A′(1) spectral feature accords with the population of several different electronic excited states over the ensemble of excited **Rebpy** molecules. It appears the that simultaneous population of two (or more) different excited states persists at least up to 5-10 ps or even longer. The shape of the excited-state A′(1) v(C≡O) band remains asymmetric in spectra measured at long time delays, for example 100 ps (Figure 12) but the low-wavenumber shoulder is weak. It appears that higher electronic excited state(s) remain populated to a small extent even at these long times. In addition, two combination bands of bpy vibrations likely contribute to the weak shoulder as well, but their combined calculated intensity (2.5 % of the A′(1) intensity) is rather small.[76] It should be noted that the time-evolving composed band-shape of the excited-state A′(1) feature have been observed for many neutral and cationic Re(I) tricarbonyl polypyridine complexes with a predominantly ^{3}MLCT lowest excited state in different media.[13,29,31,77,78] Simultaneous population of several electronic excited states persistent at least on a ps timescale thus appears to be a general feature of this class of complexes, in agreement with nonadiabatic dynamics simulations of **Rebpy** as well as $[\text{Re}(\text{im})(\text{CO})_3(\text{phen})]^+$.[14]

TRIR spectra also show an interesting solvent-dependence (Figure 12). The band shapes of 150-fs and 650-700-fs spectra agree with a broader distribution of populated excited-states in ACN than in DMSO (Figure 5 shows higher T2 and S1 populations in ACN, at the expense of T1). In ACN, the time–wavenumber map shows a large "instantaneous" shift of the A′(1) band to higher wavenumbers upon excitation (a difference between the blue and red signals close to $t = 0$) followed by a small dynamic shift. In contrast, the "instantaneous" shift in DMSO is small but followed by a large dynamic shift taking place within the first 10 ps. This different behavior can be related to larger initial structural changes calculated in ACN (hence large "instantaneous" spectral shift) than in DMSO (Figure 8). Apparently, most of the excited-induced structural changes in DMSO involve slower solvation changes and adjusting solute-solvent interactions. Later-time solvation dynamics and TRIR temporal evolution are currently under investigation in our labs, using results of nonadiabatic dynamics as a convenient starting point.

4 Conclusions

Nonadiabatic excited-state dynamics simulations of **Rebpy** suggest that subpicosecond excited-state dynamics of **Rebpy** can be
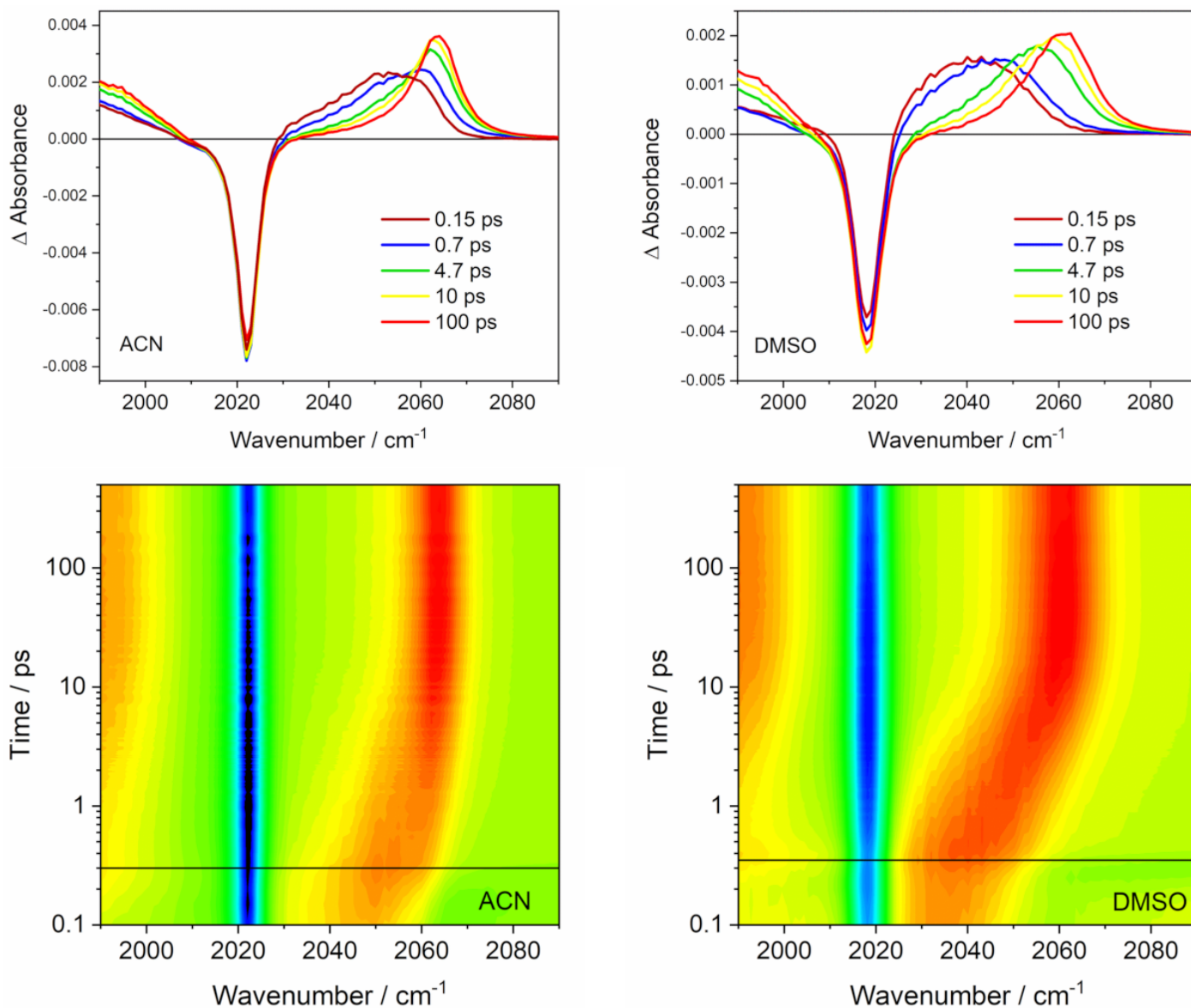
Fig. 12 Difference TRIR spectra of Rebpy in ACN (left) and DMSO (right) in the A'(1) ν(C≡O) range measured after 380 nm, ~100 fs laser–pulse excitation. Top: selected overlaid spectra. The negative band corresponds to depleted GS population, photoproduced excited-state features appear as positive signals. Bottom: time vs. wavenumber maps. Negative (bleach) features in blue, positive in red. The horizontal black line approximately denotes the time 0.

understood in terms of temporal evolution of four spin-mixed excited states that lasts longer than our simulation length of 800 fs. At this time, the lowest excited state is populated only by about 25 % in both ACN and DMSO. Population of higher excited states depends slightly on the solvent (Figure 3). A similar picture emerges in the spin-free representation that describes the excited-state evolution mostly in terms of two single and three triplet excited states whose population evolves and redistributes in hundreds of femtoseconds, probably well into the ps time range (Figure 5). ISC (defined as a conversion of total singlet to total triplet population) occurs in two phases: "fast" (< 10 fs) ISC driven by

spin-orbit wavepacket relaxation[14] and a "slow" ISC that occurs with about 800 fs (ACN) and 1000 fs (DMSO) time constants, driven by IVR, structural, and solvational changes. This ISC mechanism is qualitatively similar to that proposed[14] for [Re(im)(CO)₃-(phen)]⁺ but with two important quantitative differences: the "fast" ISC in **Rebpy** is much less efficient (20 % vs. 70 %) and the "slow" ISC component is considerably slower (ca. 1000 vs. 420 fs). Intramolecular structural changes after excitation were calculated to occur mostly within the first 200 fs after excitation while solvation dynamics remain important at longer timescales. DMSO appears to restrict the extent of the initial intramolecu-

lar restructuring. Additionally, coherent oscillations of several normal coordinates were uncovered to occur during the "slow" ISC phase. In the computational framework used, they represent a classical analogue of temporal evolution of a vibrational wavepacket.

Nonadiabatic simulations have important experimental implications. They match time-resolved fluorescence spectra and decay kinetics measured in MeCN [11–13] but change the interpretation: Femtosecond **Rebpy** fluorescence decay kinetics is not solely attributable to decaying population of fluorescent excited state(s) as the oscillator strength diminishes in the course of intramolecular structural changes and relaxation of the solvent environment. Populations and oscillator-strength effects are interrelated and hard to disentangle. (Detailed measurement of emission-wavelength dependence of the decay kinetics could provide some insight.) Changes of oscillator strength in the course of excited-state relaxation likely is a general effect that can extend to pico- and nanosecond time domains in slow-relaxing complex media such as ionic liquids or proteins. [77–79] Results of our nonadiabatic simulations also qualitatively match femtosecond evolution of Raman features observed in **Rebpy** FSRS spectra, [70] that are now attributable to the initial restructuring during the "slow" ISC phase.

The theoretical prediction that several different excited states are populated simultaneously in the excited ensemble on femtosecond and early picosecond timescales is supported by the shape of the highest $\nu(C{\equiv}O)$ band in TRIR spectra that envelops at least two gaussian peaks. This result has to be considered when interpreting ultrafast photoinduced electron transfer (ET) reactions of Re(I) tricarbonyl polypyridine complexes, either in solvent cages as in photocatalyzed CO_2 reduction [34] or in donor-acceptor assemblies. ET will occur in parallel from several different electronic excited states whose energies (and, hence, ET driving forces) span a broad range and change with time (Figure S14). This would lead to complicated ET kinetics. Indeed, photooxidation of tryptophan in azurin mutants by a covalently attached $[Re(im)(CO)_3(4,7\text{-}Me_2\text{-}phen)]^+$ sensitizer shows multi-exponential kinetics attributable to several parallel ET and relaxation steps. [35–37,72,80] We expect similar behavior for currently investigated Rebpy-based covalent donor-acceptor systems and photocatalysts.

Conflicts of interest

There are no conflicts to declare.

Notes and references

1 O. Bräm, F. Messina, A. M. El-Zohry, A. Cannizzo and M. Chergui, *Chemical Physics*, 2012, **393**, 51–57.

2 M. Chergui, *Dalton Transactions*, 2012, **41**, 13022–13029.

3 M. Chergui, *Accounts of Chemical Research*, 2015, **48**, 801–808.

4 O. Bräm, A. Cannizzo and M. Chergui, *Physical Chemistry Chemical Physics*, 2012, **14**, 7934–7937.

5 A. Cannizzo, F. Van Mourik, W. Gawelda, G. Zgrablic, C. Bressler and M. Chergui, *Angewandte Chemie - International Edition*, 2006, **45**, 3174–3176.

6 O. Bräm, F. Messina, E. Baranoff, A. Cannizzo, M. K. Nazeeruddin and M. Chergui, *Journal of Physical Chemistry C*, 2013, **117**, 15958–15966.

7 E. Pomarico, M. Silatani, F. Messina, O. Braem, A. Cannizzo, E. Barranoff, J. H. Klein, C. Lambert and M. Chergui, *Journal of Physical Chemistry C*, 2016, **120**, 16459–16469.

8 F. Messina, E. Pomarico, M. Silatani, E. Baranoff and M. Chergui, *Journal of Physical Chemistry Letters*, 2015, **6**, 4475–4480.

9 A. Vlček, *Topics in Organometallic Chemistry*, 2010, **29**, 73–114.

10 A. Kumar, S. S. Sun and A. J. Lees, *Topics in Organometallic Chemistry*, SPRINGER-VERLAG BERLIN, HEIDELBERGER PLATZ 3, D-14197 BERLIN, GERMANY, 2010, vol. 29, pp. 37–

71.

11 A. Cannizzo, A. M. Blanco-Rodríguez, A. E. Nahhas, J. Šebera, S. Záliš, A. Vlček and M. Chergui, *Journal of the American Chemical Society*, 2008, **130**, 8967–8974.

12 A. E. Nahhas, A. Cannizzo, F. V. Mourik, A. M. Blanco-Rodríguez, S. Záliš, A. Vlček and M. Chergui, *Journal of Physical Chemistry A*, 2010, **114**, 6361–6369.

13 A. El Nahhas, C. Consani, A. M. Blanco-Rodríguez, K. M. Lancaster, O. Braem, A. Cannizzo, M. Towrie, I. P. Clark, S. Záliš, M. Chergui and A. Vlček, *Inorganic Chemistry*, 2011, **50**, 2932–2943.

14 S. Mai and L. González, *Chemical Science*, 2019, **10**, 10405–10411.

15 J. P. Zobel and L. González, *JACS Au*, 2021, **1**, 1116–1140.

16 H. Takeda and O. Ishitani, *Coordination Chemistry Reviews*, 2010, **254**, 346–354.

17 R. Heydová, E. Gindensperger, R. Romano, J. Sýkora, A. Vlček, S. Záliš and C. Daniel, *Journal of Physical Chemistry A*, 2012, **116**, 11319–11329.

18 A. M. B. Rodríguez, A. Gabrielsson, M. Motevalli, P. Matousek, M. Towrie, J. Sebera, S. Záliš and A. Vlček, *Journal of Physical Chemistry A*, 2005, **109**, 5016–5025.

19 A. El Nahhas, R. M. Van Der Veen, T. J. Penfold, V. T. Pham, F. A. Lima, R. Abela, A. M. Blanco-Rodriguez, S. Záliš, A. Vlček, I. Tavernelli, U. Rothlisberger, C. J. Milne and M. Chergui, *Journal of Physical Chemistry A*, 2013, **117**, 361–369.

20 S. Záliš, C. J. Milne, A. El Nahhas, A. M. Blanco-Rodríguez, R. M. Van Der Veen and A. Vlček, *Inorganic Chemistry*, 2013, **52**, 5775–5785.

21 S. Mai, H. Gattuso, M. Fumanal, A. Muñoz-Losa, A. Monari, C. Daniel and L. González, *Physical Chemistry Chemical Physics*, 2017, **19**, 27240–27250.

22 J. Eng, C. Gourlaouen, E. Gindensperger and C. Daniel, *Accounts of Chemical Research*, 2015, **48**, 809–817.

23 M. Fumanal, E. Gindensperger and C. Daniel, *Journal of Chemical Theory and Computation*, 2017, **13**, 1293–1306.

24 Y. Harabuchi, J. Eng, E. Gindensperger, T. Taketsugu, S. Maeda and C. Daniel, *Journal of Chemical Theory and Computation*, 2016, **12**, 2335–2345.

25 M. Fumanal, F. Plasser, S. Mai, C. Daniel and E. Gin-

densperger, *Journal of Chemical Physics*, 2018, **148**, 124119.

26 C. Gourlaouen, J. Eng, M. Otsuka, E. Gindensperger and C. Daniel, *Journal of Chemical Theory and Computation*, 2015, **11**, 99–110.

27 C. Daniel, *Physical Chemistry Chemical Physics*, 2021, **23**, 43–58.

28 J. B. Asbury, Y. Wang and T. Lian, *Bulletin of the Chemical Society of Japan*, 2002, **75**, 973–983.

29 D. J. Liard, M. Busby, P. Matousek, M. Towrie and A. Vlček, *Journal of Physical Chemistry A*, 2004, **108**, 2363–2369.

30 V. A. Lenchenkov, C. She and T. Lian, *Journal of Physical Chemistry B*, 2004, **108**, 16194–16200.

31 A. M. Blanco-Rodríguez, M. Towrie, J. P. Collin, S. Záli and A. Vlček, *Dalton Transactions*, 2009, 3941–3949.

32 L. M. Kiefer, J. T. King and K. J. Kubarych, *Accounts of Chemical Research*, 2015, **48**, 1123–1130.

33 L. M. Kiefer and K. J. Kubarych, *Journal of Physical Chemistry A*, 2015, **119**, 959–965.

34 L. M. Kiefer and K. J. Kubarych, *Chemical Science*, 2018, **9**, 1527–1533.

35 C. Shih, A. K. Museth, M. Abrahamsson, A. M. Blanco-Rodriguez, A. J. Di Bilio, J. Sudhamsu, B. R. Crane, K. L. Ronayne, M. Towrie, A. Vlček, J. H. Richards, J. R. Winkler and H. B. Gray, *Science*, 2008, **320**, 1760–1762.

36 K. Takematsu, H. Williamson, A. M. Blanco-Rodríguez, L. Sokolová, P. Nikolovski, J. T. Kaiser, M. Towrie, I. P. Clark, A. Vlček, J. R. Winkler and H. B. Gray, *Journal of the American Chemical Society*, 2013, **135**, 15515–15525.

37 K. Takematsu, H. R. Williamson, P. Nikolovski, J. T. Kaiser, Y. Sheng, P. Pospíšil, M. Towrie, J. Heyda, D. Hollas, S. Záliš, H. B. Gray, A. Vlček and J. R. Winkler, *ACS Central Science*, 2019, **5**, 192–200.

38 E. D. Olmon, P. A. Sontz, A. M. Blanco-Rodríguez, M. Towrie, I. P. Clark, A. Vlček and J. K. Barton, *Journal of the American Chemical Society*, 2011, **133**, 13718–13730.

39 D. A. Case, K. Belfon, I. Y. Ben-Shalom, S. R. Brozell, D. S. Cerutti, T. E. Cheatham, V. W. D. Cruzeiro, T. A. Darden, R. E. Duke, G. Giambasu, M. K. Gilson, H. Gohlke, A. W. Goetz, R. Harris, S. Izadi, S. A. Izmailov, K. Kasavajhala, A. Kovalenko, R. Krasny, D. M. York and P. A. Kollman, *AMBER 2020*, 2020.

40   H. J. Berendsen, J. P. Postma, W. F. Van Gunsteren, A. Dinola and J. R. Haak, *The Journal of Chemical Physics*, 1984, **81**, 3684–3690.

41   J. Wang, R. M. Wolf, J. W. Caldwell, P. A. Kollman and D. A. Case, *Journal of Computational Chemistry*, 2004, **25**, 1157–1174.

42   C. I. Bayly, P. Cieplak, W. D. Cornell and P. A. Kollman, *Journal of Physical Chemistry*, 1993, **97**, 10269–10280.

43   I. S. Ufimtsev and T. J. Martinez, *Journal of Chemical Theory and Computation*, 2009, **5**, 2619–2628.

44   A. V. Titov, I. S. Ufimtsev, N. Luehr and T. J. Martinez, *Journal of Chemical Theory and Computation*, 2013, **9**, 213–221.

45   C. Song, L. P. Wang and T. J. Martínez, *Journal of Chemical Theory and Computation*, 2016, **12**, 92–106.

46   S. Grimme, J. Antony, S. Ehrlich and H. Krieg, *Journal of Chemical Physics*, 2010, **132**, 154104.

47   S. Grimme, S. Ehrlich and L. Goerigk, *Journal of Computational Chemistry*, 2011, **32**, 1456–1465.

48   J. C. Tully, *The Journal of Chemical Physics*, 1990, **93**, 1061–1071.

49   S. Mai, M. Richter, M. Heindl, M. F. S. J. Menger, A. Atkins, M. Ruckenbauer, F. Plasser, L. M. Ibele, S. Kropf, M. Oppel, P. Marquetand and L. González, *SHARC2.1: Surface Hopping Including Arbitrary Couplings — Program Package for Non-Adiabatic Dynamics*, sharc-md.org, 2019, `http://sharc-md.org`.

50   J. A. Rackers, Z. Wang, C. Lu, M. L. Laury, L. Lagardère, M. J. Schnieders, J. P. Piquemal, P. Ren and J. W. Ponder, *Journal of Chemical Theory and Computation*, 2018, **14**, 5273–5289.

51   C. Van Wüllen, *Journal of Chemical Physics*, 1998, **109**, 392–399.

52   F. Weigend and R. Ahlrichs, *Physical Chemistry Chemical Physics*, 2005, **7**, 3297–3305.

53   M. Bühl, C. Reimann, D. A. Pantazis, T. Bredow and F. Neese, *Journal of Chemical Theory and Computation*, 2008, **4**, 1449–1459.

54   D. A. Pantazis and F. Neese, *Journal of Chemical Theory and Computation*, 2011, **7**, 677–684.

55   G. Granucci, M. Persico and A. Zoccante, *Journal of Chemical Physics*, 2010, **133**, 134111.

56   F. Plasser, M. Ruckenbauer, S. Mai, M. Oppel, P. Marquetand and L. González, *Journal of Chemical Theory and Computation*, 2016, **12**, 1207–1219.

57   S. Mai, P. Marquetand and L. González, *International Journal of Quantum Chemistry*, 2015, **115**, 1215–1231.

58   A. M. Blanco-Rodríguez, H. Kvapilová, J. Sýkora, M. Towrie, C. Nervi, G. Volpi, S. Záliš and A. Vlček, *Journal of the American Chemical Society*, 2014, **136**, 5963–5973.

59   S. Mai and L. González, *Angewandte Chemie - International Edition*, 2020, **59**, 16832–16846.

60   A. Vlček and S. Záliš, *Coordination Chemistry Reviews*, 2007, **251**, 258–287.

61   K. Kalyanasundaram, *Journal of the Chemical Society, Faraday Transactions 2: Molecular and Chemical Physics*, 1986, **82**, 2401–2415.

62   B. Lin and B. M. Pettitt, *Journal of Chemical Physics*, 2011, **134**, 2011–2013.

63   P. K. Mehrotra and D. L. Beveridge, *Journal of the American Chemical Society*, 1980, **102**, 4287–4294.

64   M. L. Horng, J. A. Gardecki, A. Papazyan and M. Maroncelli, *Journal of Physical Chemistry*, 1995, **99**, 17311–17337.

65   D. Brinks, F. D. Stefani, F. Kulzer, R. Hildner, T. H. Taminiau, Y. Avlasevich, K. Müllen and N. F. Van Hulst, *Nature*, 2010, **465**, 905–908.

66   E. R. Hosler and S. R. Leone, *Physical Review A - Atomic, Molecular, and Optical Physics*, 2013, **88**, 1–7.

67   A. H. Zewail, *Journal of Physical Chemistry A*, 2000, **104**, 5660–5694.

68   Z. Wei, J. Li, L. Wang, S. T. See, M. H. Jhon, Y. Zhang, F. Shi, M. Yang and Z. H. Loh, *Nature Communications*, 2017, **8**, 4–10.

69   M. Rebholz, T. Ding, V. Despré, L. Aufleger, M. Hartmann, K. Meyer, V. Stooß, A. Magunia, D. Wachs, P. Birk, Y. Mi, G. D. Borisova, C. D. C. Castanheira, P. Rupprecht, G. Schmid, K. Schnorr, C. D. Schröter, R. Moshammer, Z. H. Loh, A. R. Attar, S. R. Leone, T. Gaumnitz, H. J. Wörner, S. Roling, M. Butz, H. Zacharias, S. Düsterer, R. Treusch, G. Brenner, J. Vester, A. I. Kuleff, C. Ott and T. Pfeifer, *Physical Review X*, 2021, **11**, 31001.

70   M. Pižl, A. Picchiotti, M. Rebarz, N. Lenngren, L. Yingliang, S. Záliš, M. Kloz and A. Vlček, *Journal of Physical Chemistry A*, 2020, **124**, 1253–1265.

71 A. Vlček, *Topics in Organometallic Chemistry*, Springer Berlin Heidelberg, Berlin, Heidelberg, 2010, vol. 29, pp. 73–114.

72 A. Vlček, H. Kvapilová, M. Towrie and S. Záliš, *Accounts of Chemical Research*, 2015, **48**, 868–876.

73 D. M. Dattelbaum, K. M. Omberg, J. R. Schoonover, R. L. Martin and T. J. Meyer, *Inorganic Chemistry*, 2002, **41**, 6071–6079.

74 D. M. Dattelbaum, K. M. Omberg, P. J. Hay, N. L. Gebhart, R. L. Martin, J. R. Schoonover and T. J. Meyer, *Journal of Physical Chemistry A*, 2004, **108**, 3527–3536.

75 M. W. George, F. P. Johnson, J. R. Westwell, P. M. Hodges and J. J. Turner, *Journal of the Chemical Society, Dalton Transactions*, 1993, 2977–2979.

76 H. Kvapilová, A. Vlček, V. Barone, M. Biczysko and S. Záliš, *Journal of Physical Chemistry A*, 2015, **119**, 10137–10146.

77 A. M. Blanco-Rodríguez, K. L. Ronayne, S. Záliš, J. Sýkora, M. Hof and A. Vlèek, *Journal of Physical Chemistry A*, 2008, **112**, 3506–3514.

78 A. M. Blanco-Rodríguez, M. Busby, K. Ronayne, M. Towrie, C. Grădinaru, J. Sudhamsu, J. Sýkora, M. Hof, S. Záliš, A. J. Di Bilio, B. R. Crane, H. B. Gray and A. Vlček, *Journal of the American Chemical Society*, 2009, **131**, 11788–11800.

79 P. Pospíšil, J. Sýkora, K. Takematsu, M. Hof, H. B. Gray and A. Vlček, *Journal of Physical Chemistry B*, 2020, **124**, 788–797.

80 A. M. Blanco-Rodríguez, A. J. Di Bilio, C. Shih, A. K. Museth, I. P. Clark, M. Towrie, A. Cannizzo, J. Sudhamsu, B. R. Crane, J. Sýkora, J. R. Winkler, H. B. Gray, S. Záliš and A. Vlček, *Chemistry - A European Journal*, 2011, **17**, 5350–5361.